

Many universality classes in an interface model restricted to non-negative heightsPeter Grassberger^{1,2}, Deepak Dhar³, and P. K. Mohanty⁴¹*JSC, FZ Jülich, D-52425 Jülich, Germany*²*MPI for the Physics of Complex Systems, D-01187 Dresden, Germany*³*Indian Institute of Science Education and Research, Dr. Homi Bhabha Road, Pune 411 008, India*⁴*Indian Institute of Science Education and Research, Mohanpur, Nadia 741 246, Kolkata, India*

(Received 27 December 2022; accepted 21 March 2023; published 18 April 2023; corrected 25 April 2023)

We present a simple one-dimensional stochastic model with three control parameters and a surprisingly rich zoo of phase transitions. At each (discrete) site x and time t , an integer $n(x, t)$ satisfies a linear interface equation with added random noise. Depending on the control parameters, this noise may or may not satisfy the detailed balance condition, so that the growing interfaces are in the Edwards-Wilkinson or in the Kardar-Parisi-Zhang universality class. In addition, there is also a constraint $n(x, t) \geq 0$. Points x where $n > 0$ on one side and $n = 0$ on the other are called “fronts.” These fronts can be “pushed” or “pulled,” depending on the control parameters. For pulled fronts, the lateral spreading is in the directed percolation (DP) universality class, while it is in a different universality class for pushed fronts, and another universality class in between. In the DP case, the activity at each active site can in general be arbitrarily large, in contrast to previous realizations of DP. Finally, we find two different types of transitions when the interface detaches from the line $n = 0$ (with $\langle n(x, t) \rangle \rightarrow \text{const}$ on one side, and $\rightarrow \infty$ on the other), again with new universality classes. We also discuss a mapping of this model to the avalanche propagation in a directed Oslo rice pile model in specially prepared backgrounds.

DOI: [10.1103/PhysRevE.107.044112](https://doi.org/10.1103/PhysRevE.107.044112)**I. INTRODUCTION**

Simple low-dimensional stochastic models—either in equilibrium or out of equilibrium—have been at the core of statistical physics for a very long time. One reason is that they can—if they are sufficiently simple and “natural”—be used for bewildering wide ranges of phenomena. We might just mention the Ising model that was conceived as a model for magnets but has found applications in liquid-gas critical points [1] and in social dynamics [2], to mention just a few. Another one is random walks and modifications thereof, which are relevant not only for Brownian motion but also for finance [3] and for polymer configurations [4]. As final examples we have ordinary and directed percolation (DP). Both are basic models for the spreading of epidemics [5], although the former has also found application in the sol-gel transition [6], while the latter was—under the name of Reggeon field theory—once considered as a core model for ultrarelativistic hadron collisions [7,8].

This property of a model being applicable in a wide variety of contexts is particularly pronounced in one dimension, where particle, spin, and interface models can be mapped onto each other. But this mapping can exist also in higher dimensions, where it was observed by Paczuski and Boettcher [9] that “sandpile” models [10] can be mapped exactly onto models for interface depinning.

In the present paper we shall introduce and discuss a very simple one-dimensional (1D) fully discrete model. We shall formulate it as a stochastic evolution model of an interface with pointlike pinning centers and a lower barrier below which the interface cannot go. This interface can get pinned at the barrier, and when it detaches, it can either grow laterally (i.e.,

in more and more regions the height above the barrier changes from zero to >0) or in height. These two types of transitions are associated with different universality classes. We will also show that the model can also be interpreted as a model for the spreading of avalanches in specially prepared backgrounds in the directed version [11] of the Oslo rice pile model [12].

The lateral spreading of detached regions can—depending on the control parameters—be in the universality class of DP. But, while activity in the active phase is binary in all previous realizations of DP (sites can either be dead or active), in the present model it can be active to varying degrees, and this degree of activity is a slow variable. While DP can be used as a model for infections where reproduction of infectants is so fast that a classification of individuals as healthy or infected is sufficient [5], it is not suitable for some helminth infections (e.g., with *Ascaris lumbricoides* [13–15]) where parasites cannot reproduce within the infected individual, and the number of parasites in an individual is a slowly varying relevant parameter. Although we shall not go into detail, it is clear that our model is thus more suitable as a model of helminth infections than standard DP.

A formal definition of the model is given in the next section. In Sec. III we will discuss the sector where the interface is so far above the barrier that the latter is not felt. In that case the model shows—depending on parameters—scaling in the Kardar-Parisi-Zhang (KPZ) [16] and Edwards-Wilkinson (EW) [17] universality classes, respectively. Interfaces which stay close to the barrier, i.e., for which $\langle n(x, t) \rangle \rightarrow \text{const} < \infty$ for $t \rightarrow \infty$ (or, in the tent phase, where $\langle n(x, t) \rangle$ remains bounded by a time-independent constant for most x at any t), are discussed in Sec. IV, while the transition between interfaces attached to the barrier to interfaces which become

detached, i.e., for which $\langle n(x, t) \rangle \rightarrow \infty$ for $t \rightarrow \infty$, is treated in Sec. V. Finally, a mapping to propagation of avalanches in the directed Oslo rice pile model on specially prepared backgrounds is discussed in Sec. VI. Section VII summarizes our results.

II. DEFINITION OF THE MODEL

We consider a 1D lattice of size $2L$ with periodic boundary conditions and synchronous updating. At time $t = 0$ a non-negative integer $n(x, t) \geq 0$ is attached to each even site x . Odd (even) sites are updated only for odd (even) times, with the evolution rule

$$n(x, t + 1) = \frac{1}{2}n_{\text{in}}(x, t + 1) + \eta[n_{\text{in}}(x, t + 1)], \quad (1)$$

where

$$n_{\text{in}}(x, t + 1) = n(x - 1, t) + n(x + 1, t). \quad (2)$$

Here $\eta(n_{\text{in}})$ is the simplest nontrivial noise term that depends only locally on n , preserves the non-negativity and integer nature of $n(x, t)$, and leaves the zero state $n(x, t) = 0$ invariant. This leaves us with

$$\eta(n) = \begin{cases} 0 & \text{for } n = 0 \\ \pm \frac{1}{2} & \text{with probabilities } (q, 1 - q) \text{ for odd } n \\ \pm 1, 0 & \text{with probabilities } (p_{\pm 1}, p_0) \text{ for even } n > 0 \end{cases}, \quad (3)$$

where $p_{-1} + p_0 + p_1 = 1$.

In the following we shall usually interpret $n(x, t)$ as the height of an interface without overhangs, although we shall also mention some other interpretations. We shall consider only initial conditions where $n(x, t)$ is either flat or has finite variance, i.e., we shall consider neither interfaces which have infinite roughness already initially nor circular interfaces as in the Eden model [18].

Before going on, we point out that the average instantaneous velocity of an interface $\mathcal{I}_{t-1} = \{n(x, t - 1)\}$,

$$v(a, t) = \frac{1}{L} \left[\sum_{x:x+t=\text{even}} \langle n(x, t) \rangle - \sum_{x:x+t=\text{odd}} n(x, t - 1) \right], \quad (4)$$

can be calculated from $m_{\text{odd}}(t)$ and $m_{\text{even}}^+(t)$, which are the number of sites where $n_{\text{in}}(x, t)$ is odd or even and positive. Indeed, it follows straightforwardly from Eqs. (1) and (3) that

$$v(a, t) = \frac{1}{L} [(q - 1/2)\langle m_{\text{odd}}(t) \rangle + (p_1 - p_{-1})\langle m_{\text{even}}^+(t) \rangle]. \quad (5)$$

This is extremely useful in simulations, since Eq. (5) gives always smaller statistical fluctuations than the “naive” use of Eq. (4), in particular when q is close to $1/2$ [19]. The reason is that relative fluctuations in $m_{\text{odd}}(t)$ and $m_{\text{even}}^+(t)$ are much less than in $\eta(x, t)$. In fact, Eq. (5) is a variance-reduced estimator similar to those used in [20–23]. Its use was crucial for obtaining the results of [19] and of the present paper.

III. INTERFACES WHERE $n(x, t)$ IS STRICTLY POSITIVE FOR ALL x AND t

If the interface is everywhere strictly above the barrier, the barrier at $n = 0$ is ineffective, and it remains so, if the mean velocity of the interface is positive, provided that statistical fluctuations don’t push it down to $n = 0$. Assume that the p_i ’s are such that $v > 0$ for $q = 1$. Then the barrier is ineffective for all times, if we started sufficiently high so that these fluctuations can be neglected.

As we decrease q , keeping the p ’s constant, the velocity can only decrease. If it becomes negative, the moving interface eventually comes in contact with the barrier. We call this value of q where $v = 0$ the critical value $q_{c,a}(p_0, p_1)$, where “a” stands for absence of barrier. If we decrease q further, the interface will finally, i.e., for sufficiently small q , get stuck at $n = 0$. But there might be an interval of q between $q_{c,a}(p_0, p_1)$ and a second threshold $q_{c,b}(p_0, p_1)$ (where “b” stands for barrier) where it fluctuates above $n = 0$, without getting completely absorbed or being able to detach completely. Indeed, $q_{c,b}$ might be either smaller or larger than $q_{c,a}$, depending on the values of p_0 and p_1 .

In this section we will discuss only the values of $q_{c,a}$ and the behavior when the barrier can be neglected. Values of $q_{c,b}$ and the behavior when the interface actually does interact with the barrier will be discussed in Secs. IV and V.

A plot of the numerically determined contour lines $q_{c,a} = 0, 0.1, 0.2, \dots, 1.0$ is given in Fig. 1.

The up-down symmetry of this plot follows from the invariance

$$\{p_1, q, n(x, t)\} \leftrightarrow \{p_{-1}, 1 - q, \text{const} - n(x, t)\}. \quad (6)$$

At the right-hand side of Fig. 1, each contour line ends tangentially at one of the two phase boundaries $|p_1 - p_{-1}| = 1 - p_0$ at a finite value of p_0 .

For finite system size L or when the interface is infinitely high above the barrier, we can also consider tilted initial conditions,

$$n(x, 0) = \text{const} + ax. \quad (7)$$

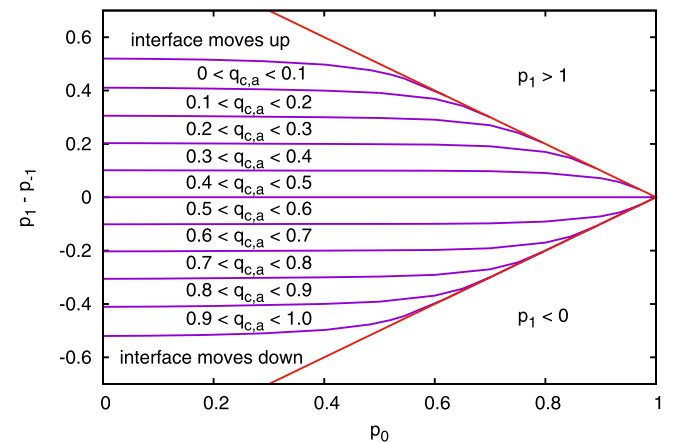


FIG. 1. Contour lines for the threshold values $q_{c,a} = 0, 0.1, 0.2, \dots, 1.0$, plotted with p_0 on the x axis vs $p_1 - p_{-1}$ on the y axis. The triangular regions at the right are unphysical with $p_1 < 0$ or $p_1 > 1$.

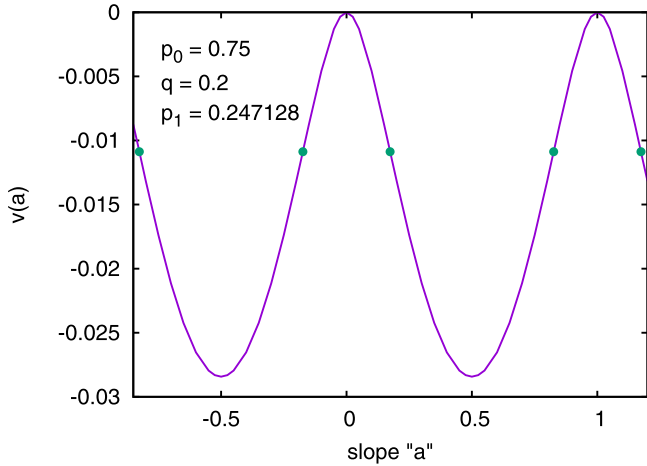


FIG. 2. Average asymptotic interface velocity for tilted interfaces with tilt a . Parameters are such that interfaces without tilt are critical, $v(0) = 0$. The curve resembles a cosine but is clearly distinct from it on closer inspection. The filled dots indicate inflection points where the curvature is zero.

In this case, the speed in general depends on the slope a . Thus also the critical values of q depend in general on a . An exception is the central line $p_1 = p - 1, q = 1/2$ in Fig. 1. Because of the symmetry (6), the average speed there is zero, and the model is thus critical for all slopes. As a consequence, we expect the roughness at criticality, and the speed near criticality, to scale according to the EW class along the central line, but according to the KPZ class everywhere else. This is indeed observed in simulations, although the scenario is somewhat delicate.

Typical values of the velocity $v(a)$ of the interface, for a fixed set of control parameters, are plotted in Fig. 2 versus the tilt a . We see that $v(a)$ is periodic with period 1. This is indeed easy to prove exactly [19]: The deterministic part of Eq. (1) gives a speed that is independent of a , and the noise is invariant under a change $a \rightarrow a + 1$. This periodic dependence of the speed on the tilt is rather unusual for models in the KPZ universality class and is responsible for the slow convergence discussed in the following (a more thorough discussion is given in [19]).

In particular, the periodicity of $v(a)$ implies the existence of inflection points in Fig. 2 where the curvature vanishes. Such points have been discussed previously in the context of KPZ [24]. As expected, at such points we also find EW scaling. But we find also deviations from the standard KPZ scenario when the curvature $v''(a)$ is small—either we are close by an inflection point, or when q is very close to $1/2$. As the curvature tends to zero, we find that the average interface velocity at large but finite t scales as [19]

$$v(t, a) \approx v(a) + \text{const}/\sqrt{t}, \tag{8}$$

which is different from both the KPZ behavior where

$$v(t, a) \approx v(a) + \text{const}/t^{2/3}, \tag{9}$$

and from EW, where there is no power-behaved correction to $v(t, a) \rightarrow v(a)$ at all. We conjecture that Eq. (8) holds exactly in the double limit ($v''(a) \rightarrow 0, t \rightarrow \infty$, in a not yet precisely

determined time range $t_1 < t < t_2$, where t_1 and t_2 depend on $v''(a)$. Our data do not rule out the possibility that t_2 is infinite in a finite range of q near q_c .

Because of the slow convergence of the velocity of the interface to its asymptotic value, it becomes difficult to pin down precisely the critical parameters where $v = 0$ and the precise values of $q_{c,b}$. These complications do not seem to affect the scenario developed in the following and do not prevent us from reaching clear conclusions in the next sections.

IV. INTERFACES TOUCHING THE BARRIER AND FINITE SEEDS: LATERAL SPREADING

Let us next consider the case where the barrier at $n = 0$ is effective, e.g., because the evolution starts from a finite “seed.” We call the seed \mathcal{S} of a simulation the set of lattice sites where $n(x, 0) > 0$, while $n(x, 0) = 0$ for all x not in \mathcal{S} . The seed can consist of a single site, of a finite interval, or of a union of finite intervals. We call the size R_0 of the seed the distance between its rightmost and leftmost points. Similarly, we denote by $R(t)$ the distance between its rightmost and leftmost points in the configuration at time t which evolved from this seed, and by $N(t)$ the integrated height, $N(t) = \sum_x n(x, t)$. We say that a configuration “survives” up to time t , if $N(t) > 0$. The probability that a configuration survives at least up to t is denoted as $P(t)$. Of course, $R(t), N(t)$, and $P(t)$ depend on \mathcal{S} . Let us denote as $P_{\infty, \mathcal{S}}$ the probability that a configuration starting from \mathcal{S} survives forever, and $q_{c,b, \mathcal{S}}(p_0, p_1)$ the largest value of q for which, at fixed (p_0, p_1) , the survival probability $P_{\infty, \mathcal{S}}$ is zero.

In addition to this survival or extinction transition there is also, in general, a second transition between the cases where the average height remains bounded (the interface is attached to the barrier $n = 0$) and where it detaches [$\langle n(t) \rangle \rightarrow \infty$]. This transition will be discussed in the next section. Here we will discuss only the case where $\langle n(t) \rangle$ stays bounded for $t \rightarrow \infty$.

It is clear that configurations can survive forever only if $N(t)$ and $R(t)$ increase beyond any limit. But that suggests also that the detailed form of the seed becomes less and less relevant for the further evolution, as time goes on. Thus we expect that the asymptotic scalings of R, N , and P are independent of \mathcal{S} , and that also $q_{c,b, \mathcal{S}}(p_0, p_1)$ does not actually depend on \mathcal{S} , as long as \mathcal{S} is finite and non-null (an analog situation prevails in DP). This was verified by extensive simulations, and the resulting critical values $q_{c,b}$ are plotted in Fig. 3 against p_0 and $p_1 - p_{-1}$. In the following, we shall call $q_{c,b}$ also the “critical values for spreading.” The extremal points where $n(x, t) > 0$ are called the left and right “fronts” of the configuration at time t .

A. Pulled versus pushed fronts

Both sets of contour lines are plotted in Fig. 4, where we also indicate by different colors the regions where $q_{c,a} > q_{c,b}$ and $q_{c,a} < q_{c,b}$. For reasons that will become clear soon, we call the former “pulled” and the latter “pushed.” There is one connected pushed region and two pulled regions. One boundary between pulled and pushed regions is the central line $q = 1/2$. The dynamics on this line satisfies detailed

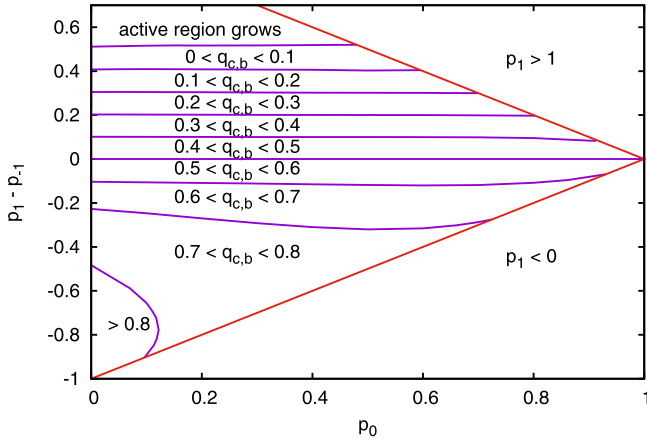


FIG. 3. Contour lines $q_{c,b} = 0, 0.1, 0.2, \dots, 1.0$ (critical values for spreading from finite seeds), plotted with p_0 on the x axis vs $p_1 - p_{-1}$ on the y axis.

balance, and the presence of a lower barrier does not break it. The other boundary, in the upper left corner of the plot, is known only numerically.

Figure 4 shows that the existence of fronts created by the lower barrier can either help or hinder the spreading of activity. If $q_{c,b} < q_{c,a}$, then for $q \in [q_{c,b}, q_{c,a}]$ a finite seed will lead (with nonzero probability) to a configuration that spreads forever laterally, while the height of an interface starting from an infinitely extended seed would decrease until it hits the barrier. This means that the front *pulls* the active configuration. If, on the contrary, $q_{c,b} > q_{c,a}$, then the active region shrinks and the activity finally dies for q in between these two critical points. This means that the front *pushes* back the activity until

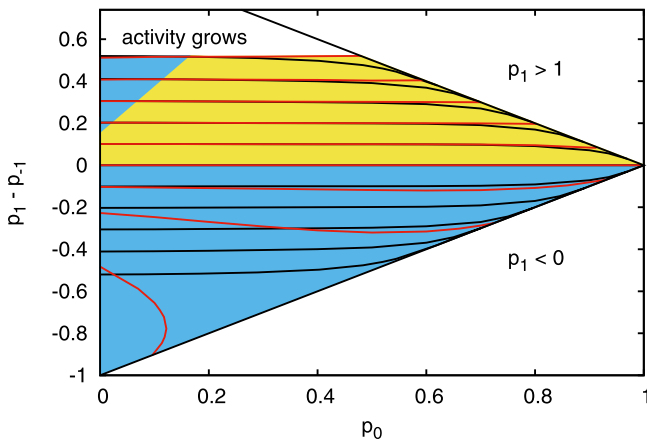


FIG. 4. Both sets of contour lines superimposed, in order to show where the finiteness of the seed enhances or hinders the proliferation of activity. The region where $q_{c,a} < q_{c,b}$ is colored yellow, while the two regions where $q_{c,a} > q_{c,b}$ are colored blue. In the blue regions fronts are pulled and the active-dead transition is in the DP class, while fronts are pushed in the yellow region and the active-dead transition is via tentlike interfaces. In the lowest part of the lower blue region (below the lowest curved black line) $q_{c,a}$ is not defined since fronts recede there for all values of q in the absence of a barrier. Thus, in that region the inequality $q_{c,a} > q_{c,b}$ is not applicable, but fronts are still pulled there.

it finally dies, although the height of an infinitely extended interface without any fronts would increase forever.

Pulled and pushed interfaces are well known from bistable media [25], from wetting phenomena (where wetting fluids correspond to pulled fronts, and nonwetting fluids lead to pushed fronts) [26], and from spatially extended chaotic systems [27].

B. Universality classes

There are at least five different universality classes for the critical dynamics of interfaces in contact with the barrier.

1. Compact DP

We find compact DP [28] for $p_0 = 1$ in addition to $p_1 = 0$ and $q = 1/2$. A particularly simple situation prevails when in addition $n(x, 0) \leq 1$ for all x , since in that case $n(x, 1) \leq 1$ also for all $t > 0$, and the model maps onto the compact DP point in the Domany-Kinzel [29] model (see Sec. III).

2. Clipped EW

The next numerically clean and theoretically well-understood case happens when infinite seeds would lead to increasing interfaces in the EW class, and fronts neither pull nor get pushed. This occurs when $q = 1/2$ and $p_1 = p_{-1}$. Since EW interfaces are Brownian, an interface between two fronts starting from a single point seed is just an arc with $n > 0$ clipped out from a Brownian curve; see Fig. 5(a). Since the fronts neither pull nor get pushed, they perform random walks in x . Thus their distance increases as $t^{1/2}$, and the average height $\langle n(x, t) \rangle$ of the nonzero part of the interface increases as $t^{1/4}$.

If events could die only because the two outer fronts annihilate, we would have $P(t) \sim t^{-1/2}$. But actually $n(x, t)$ can become zero also inside the arc, creating thereby pairs of (inner) fronts which can then annihilate later with the outer ones. The result is that actually $P(t) \sim t^{-3/4}$. As a consequence, $N(t)$ does not scale as $P(t) \times R(t) \times \langle n(x, t) \rangle \sim \text{const}$ as one would expect naively, but $N(t) \sim t^{-1/4}$. As seen from Fig. 6, all these predictions are perfectly verified by simulations at the particular point $(p_0, q) = (1/2, 1/2)$, but we found the same also along the entire line $q = 1/2$.

Both compact DP and clipped EW are unstable in the RG sense. When control parameters are perturbed such that they stay on the critical surface, they remain in their universality classes for short times and small distances, but later cross over to the more stable universality classes of DP [Fig. 5(b)] or the tent phase [Fig. 5(c), discussed in the next paragraphs. Thus DP and the tent phase are more robust, but for the very same reason they are also more difficult to analyze numerically. Unless the control parameters are carefully chosen to minimize cross-over effects (which would be analogous to the use of improved Hamiltonians in equilibrium [30,31], and which would be beyond the scope of this article), the simulations are hampered by very slow convergence due to the presence of nearby clipped EW fixed point.

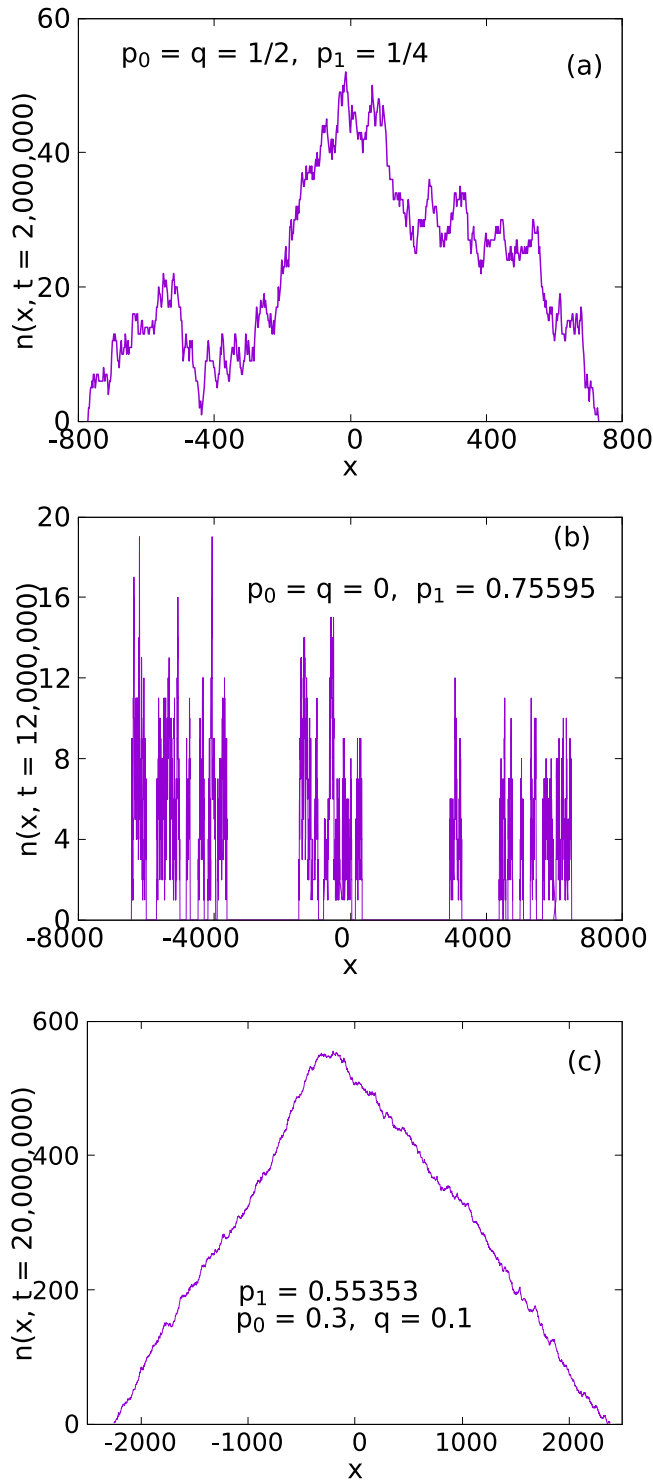


FIG. 5. Typical interfaces obtained at long times when fronts neither push nor pull (a), when they pull the active region (b), or when they push it back (c).

3. Directed percolation

The behavior is particularly simple when $p_1 = 0$ and when the initial state has $n(x, 0) \leq 1$ for all sites x . Then it is easily seen that $n(x, t) \in \{0, 1\}$ also for all later times. In this case we are left with two independent control parameters q and p_0 , and the model can be mapped exactly onto the well-known

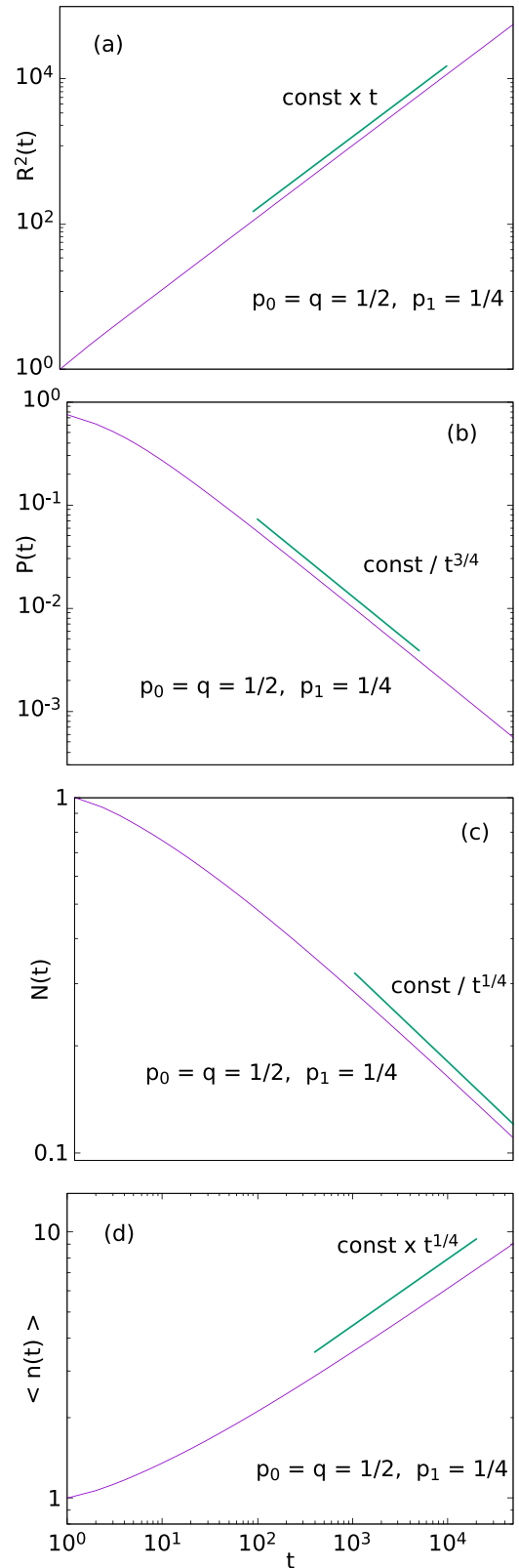


FIG. 6. Log-log plots for time-dependent observables in the clipped EW universality class: (a) random mean-squared distance of active sites from the origin; (b) probability that the interface still moves at time t ; (c) average number of active sites, i.e., of sites with $n(x, t) > 0$; and (d) average height $\langle n(x, t) \rangle$ of these sites. In all panels, the straight lines indicate the asymptotic scalings, the same set of control parameters is used, and the seed is a single point.

Domany-Kinzel (DK) cellular automaton model [29]. In the DK model, $n(x, t) = 1$ means that site x is infected at time t , while $n(x, t) = 0$ means that it is susceptible. Neighboring pairs “01” and “10” at positions $x \pm 1$ infect site x at the next time step with probability p , while pairs “11” infect it with probability p' . In the present notation, $p = q$ and $p' = p_0$. If $q = p_0$, then two infected neighbors have the same chance to infect the site between them as does a single infected neighbor. This corresponds to site DP. On the other hand, if the second infected neighbor has the same chance to infect it as the first one (provided the first neighbor was not successful), we have bond DP and $p_0 = 2q - q^2$. Finally, when $p = 1/2$, the critical behavior of the DK model is in the compact DP [28] class, which is thus also the universality class of our model for $p_1 = 0$, $q = 1/2$, and $n(x, 0) \leq 1$ for all sites x .

For arbitrary finite seeds, DP occurs whenever the front is pulled. This is the case along the boundary line $p_1 = 0$, but it also occurs in both blue regions of Fig. 4. Numerical results obtained at $p_0 = q = 0$ for the same four observables as in the previous figure are shown in Fig. 7. Here and in the following examples we do not determine the critical q for fixed p_0 and p_1 , but we fix p_0 and q and then determine $p_{1,c}$. We see clearly that the known DP critical exponents [32] hold for $p_1 = 0.75587(1)$, although the scaling sets in rather late—as was expected from the fact that there can be slow cross-overs from other unstable fixed points. Similar results were found in all regions where we expect DP scaling. Notice, however, that the activity per site [the value of $n(x, t)$] can become arbitrarily large. More precisely, at the critical surface $(n(x, t))$ tends to a finite value $n_\infty(p_0, p_1)$. For a few selected values of the control parameters, $n_\infty(p_0, p_1)$ is plotted in Fig. 8. As $p_1 \rightarrow 0$ we have $n_\infty(p_0, p_1) \rightarrow 1$, while $n_\infty(p_0, p_1)$ diverges when $p_{-1} - p_1 \rightarrow 0$, as in this limit the behavior has to cross over to clipped EW. But it diverges also when the other boundary between pulled and pushed phases (see Fig. 3) is approached.

4. The tent transition and the tent phase

A scaling very different from DP is observed when fronts try to push the activity back but are pushed out by the bulk. This transition between spreading and nonspreading phases has many features of a first-order transition, although we will avoid this terminology, which, after all, is rooted in equilibrium theory.

Plots like those in Figs. 6 and 7, but for a typical point on the tent transition manifold, are shown in Fig. 9. The first striking observation is that $P(t)$ does not seem to follow a power law at the critical point. Rather, the system seems to go through a bottle neck as t increases and one is very slightly overcritical. More precisely, $P(t)$ seems to decrease faster than with a power law, until the very few surviving “clusters” have reached a critical size, after which they grow linearly and $P(t)$ no longer decreases at all. This qualitative behavior is typical of cluster growths near critical points in first-order transitions in various systems like nucleation [33], magnetism [34], wetting [35], and coinfections [36]. This interpretation is confirmed by the other panels of Fig. 9. Figures 9(b) and 9(c) show that both $N(t)$ and $R(t)$ grow linearly with t , as soon as the bottleneck is passed. Moreover, a closer analysis shows that $N(t)/P(t) = R(t)$ up to finite

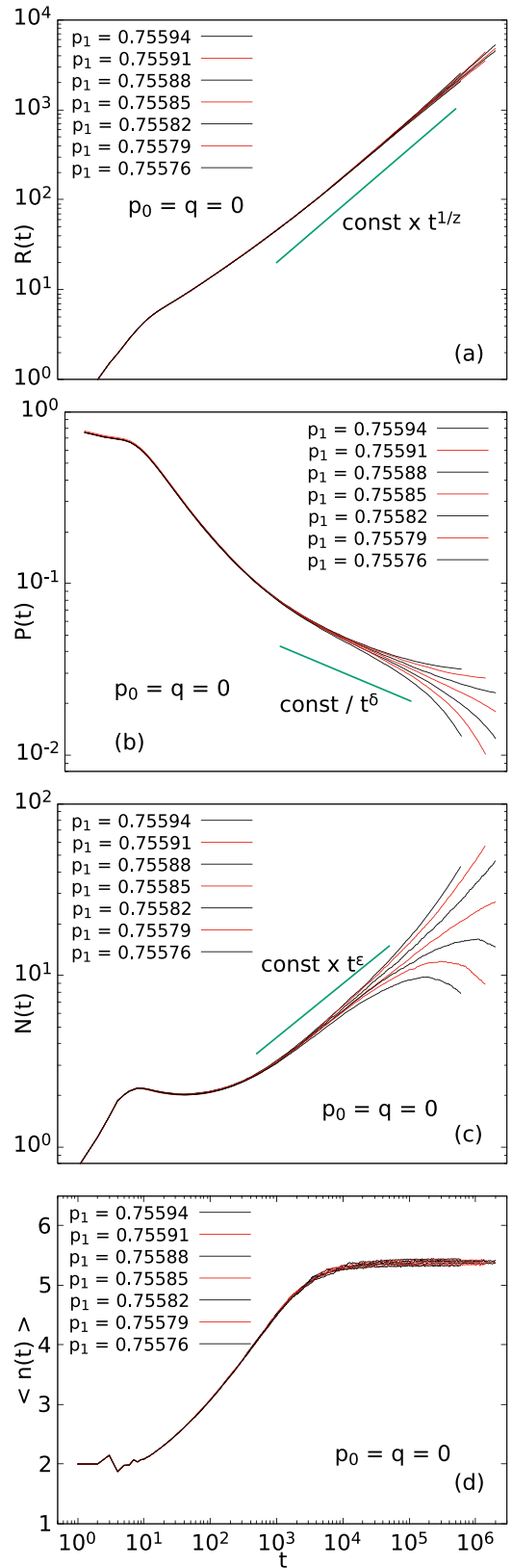


FIG. 7. The same four observables as in the previous figure, but now for a set of parameter values in the DP universality class. Again a point seed was used. In all panels [except panel (d)] the straight lines indicate the asymptotic scaling expected for DP [32]. All panels show log-log plots, except for panel (d), which is log-linear. Notice that $\langle n(x, t) \rangle = 1$ for ordinary DP.

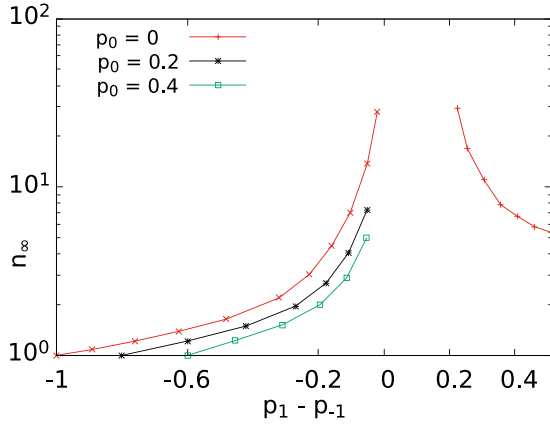


FIG. 8. Log-linear plot of asymptotic average interface heights of active sites, at three lines on the critical DP transition manifold.

(cluster) size corrections, when $q > q_{c,b}$. This is precisely what we expect if the active region is compact without any holes. Finally, Fig. 9(d) shows that the ratio between the lateral size $R(t)$ and the average $\langle n(x, t) \rangle$ of the surviving clusters tends to a constant, as expected from the tentlike shape of the asymptotic curve in Fig. 5, independent of p . What changes with the distance from the critical point is the speed of expansion. Figures 9(b) and 9(c) show that this speed increases linearly with q .

At first it might seem that it is impossible to determine precisely the transition point from simulations like those presented in Fig. 9. The curves for $P(t)$ indicate that $p_{1,c} \approx 0.4$ to 0.4007 but not more. But there is an easy way to obtain more precise estimates. First of all, Fig. 9 was, just like Figs. 6 and 7, for point seeds. Using extended and tent-shaped seeds with R_0 up to several thousands, we can avoid the bottleneck, since for such large seeds $P(t) \approx 1$ even very close to the transition point. Second, in such runs we can measure rather precisely the asymptotic speed v_∞ of (lateral and vertical) growth. Extrapolating linearly to $v_\infty = 0$ gives then the critical point. For the present case we get, e.g., $p_{1,c} = 0.40022(1)$. This is indeed how most of the simulations underlying Fig. 2 were performed.

From Fig. 9(d) we also see that $\langle n(x, t) \rangle / R(t)$ tends, for $t \rightarrow \infty$ and for all values of p_1 to the same constant,

$$\lim_{t \rightarrow \infty} \langle n(x, t) \rangle / R(t) = 0.26(1). \quad (10)$$

If, indeed, the shapes becomes triangular in this limit, then this is the asymptotic slope of the triangles. The fact that this limit is approached from below is due to statistical fluctuations which tend to round off the top of the triangles for small t and for p_1 very close to $p_{1,c}$.

Figure 9 (and many simulations at other control parameter values) confirms that surviving clusters at late times are tent shaped; see Fig. 4(c). This is easily understood. Since interfaces without fronts would be in the KPZ universality class, the velocity of tilted interfaces would depend on their tilt, such that flat interfaces move fastest. At the same time, since fronts are pushed out by the bulk and the bulk is pushed back by the fronts, statistical fluctuations at one of the front positions cannot propagate back into the interior of the cluster. Together these two observations imply that statistical fluctuations prop-

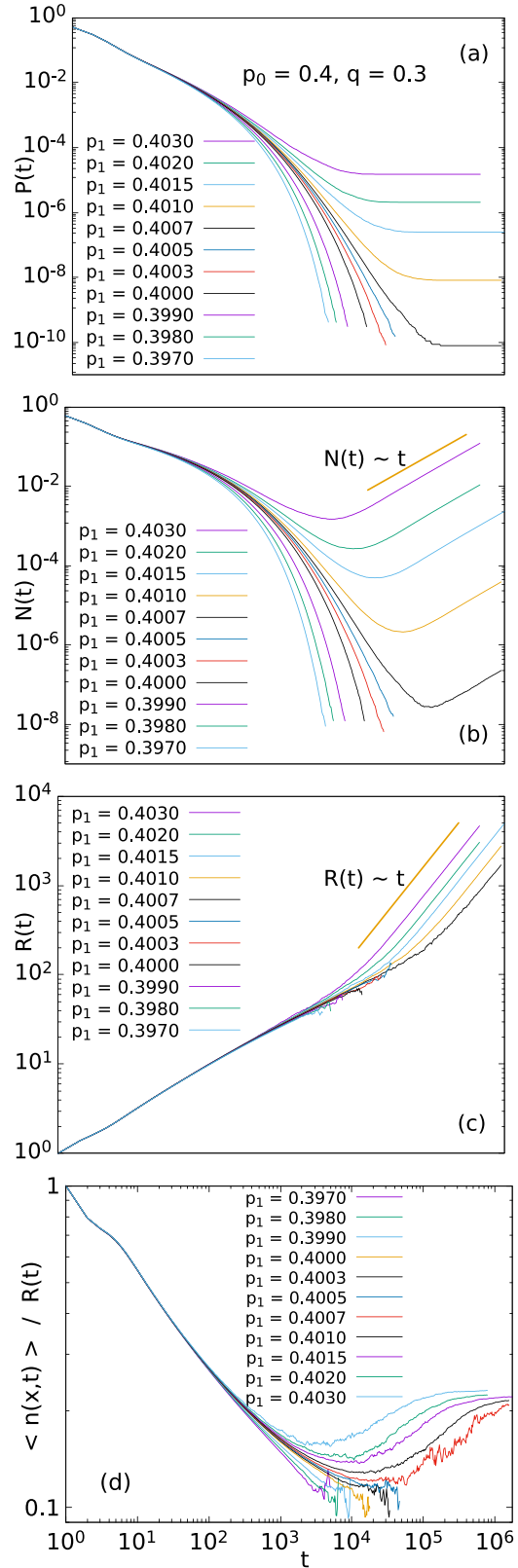


FIG. 9. Panels (a) to (c) show log-log plots of the same observables as in the first three panels of Fig. 7, but now for $p_0 = 0.4$ and $q = 0.3$ where the transition is of tent type. Again a point seed was used. In panels (b) and (c) the straight lines indicate the asymptotic scaling, which corresponds just to a linear expansion. Panel (d) shows the ratio between the average height $\langle n(x, t) \rangle$ and the average lateral size $R(t)$.

agate outward, as long as the local tilt is larger than a critical value. It is this critical tilt which then defines the slope of the triangular profiles that evolve. More precisely, let us denote the triangle slope as a_Δ . Then we have

$$q_{c,a}(a_\Delta) = q_{c,b}. \quad (11)$$

This was indeed confirmed, within measurement errors, for all tested control parameters. In particular, it was verified that $q_{c,a}(0.26) = 0.3$ for $p_0 = 0.4$ and $p_1 = 0.40022$, within the statistical errors.

A further important difference between the tent and DP transitions is that $\langle n(x,t) \rangle$ diverges (linearly) for $t \rightarrow \infty$ as soon as one has passed the tent transition, while, as we had seen, it converges to a finite value in slightly supercritical DP. It is only at a finite distance above the DP transition that interfaces detach, in a second transition, from the barrier. That second transition will be discussed in Sec. V.

5. Clipped KPZ

The next universality class is that when fronts neither are pushed nor pull, and interfaces without fronts would be in the KPZ universality class. This is realized along the short approximately straight line in Fig. 3 that cuts off the triangle in the upper left corner. In this case most of the remarks about capped EW should apply *mutatis mutandis*. But numerical verification was impossible because of the problems discussed in [19].

V. DETACHMENT TRANSITIONS OF PULLED INTERFACES FROM THE BARRIER

Let us finally discuss the critical behavior(s) at $q = q_{c,a}$, in the case where $q_{c,b} < q_{c,a}$ and where therefore fronts are pulled. In this case we have interfaces attached to the barrier for $q_{c,b} < q < q_{c,a}$, while they must be detached for $q \gg q_{c,a}$.¹ Clearly, the *detachment transition* is exactly at $q_{\text{detach}} = q_{c,a}$. Otherwise (if $q_{\text{detach}} > q_{c,a}$) we would have bistability in the interval $q_{c,a} < q < q_{\text{detach}}$: An interface which started at height $n_0 \gg 1$ would be detached forever, while one starting at finite n_0 would remain attached forever. An even stranger situation would prevail if q_{detach} depends on n_0 . In the following we shall present numerical evidence that seems to exclude such exotic behavior, and which strongly suggests that $q_{\text{detach}} = q_{c,a}$.

As seen from Fig. 4, there are two disjoint regions (both indicated in blue) where $q_{c,b} < q_{c,a}$. In the larger (lower) region, $q_{c,a} > 1/2$ and thus

$$\langle n(x,t) \rangle \sim n_\infty + c t^\alpha, \quad (12)$$

with $c > 0$ (it does not really matter whether $\alpha = 1/3$ as for proper KPZ or $\alpha \approx 1/2$ as seen effectively for $q \approx 1/2$ [19]). On the other hand, we have $c < 0$ in the smaller (lower) blue region in Fig. 4. In the first case a critical interface

¹Notice that the following discussion applies only to the part of phase space where $q_{c,a}$ is defined, thus it does not apply at the region below the lowest curve in Fig. 1. In that region, interfaces can never detach from the barrier.

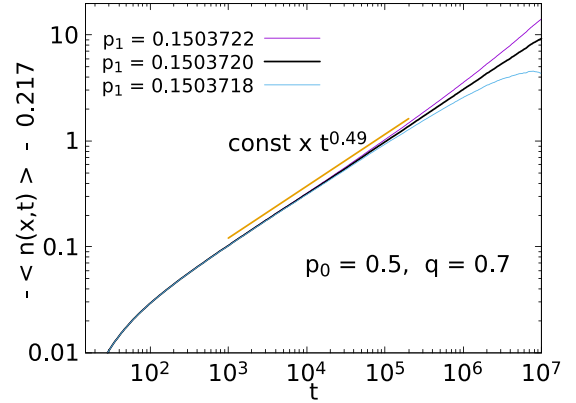


FIG. 10. Average heights for $p_1 \approx p_{1,c}$ at point 1 in absence of a barrier, plotted against t . More precisely, a log-log plot is shown of minus the average height, shifted by an amount which is chosen such that the curve for $p_1 = p_{1,c}$ is straight for the largest range.

would move towards the barrier for small t , while it would move away from it in the second case. We shall call the first “uneasy detachment,” while the second is “easy detachment.” We should expect that the effect of the barrier is different in both cases, and that we have indeed two different universality classes.

In order to decide this and to obtain critical exponents, we turn again to simulations. We choose values of p_0 and p_1 in the upper or lower blue regions of Fig. 4, and depending on them we choose $q \approx q_{c,a}$. We start each run with $n(x,t) = n_0 \geq 1$ for all even x . Although we made simulations also for $n_0 > 1$, we show only results for $n_0 = 1$. As observables we measure the average and variance of the height $n(x,t)$ as a function of t , and the height distribution $\rho(n,t)$ at fixed t . In particular we look at $\rho(0,t)$, i.e., the probability that the interface touches the barrier at any given site. In all simulations we used $L = 2^{19}$.

Although we looked also at other control parameters, we show results only for the two choices:

- (1) $(p_0, q) = (0.5, 0.7)$, where $p_{1,c} \approx 0.15$ and
- (2) $(p_0, q) = (0.1, 0.0)$, where $p_{1,c} \approx 0.71$.

Notice that we again switched from fixing p_0 and p_1 to fixing p_0 and q . As in the previous subsections this was done purely for numerical convenience, without any deeper reason. Choice 1 corresponds to uneasy detachment, while detachment is easy for choice 2.

A. Uneasy detachment

In order to obtain a precise estimate of $p_{1,c}$ at point 1, we show in Fig. 10 plots of the average interface height versus t in absence of the barrier. More precisely, we show log-log plots of $c - \langle n(x,t) \rangle$, where $c = -0.217$ is chosen such as to maximize the region where the critical curve shows a clean power law. We see indeed a perfect power law, with exponent $\alpha \approx 0.49$, [37] for $p_{1,c} = 0.15037198(10)$. Notice that the error of $p_{1,c}$ takes into account the uncertainty of α and is indeed largely dominated by it.

Results for $\langle n(x,t) \rangle$ versus t in presence of the barrier, at several values of p_1 , are shown in Fig. 11. Although there are huge corrections to it, a conventional finite-size scaling (FSS)

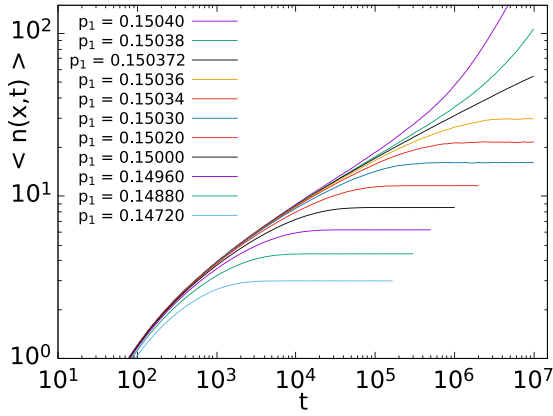


FIG. 11. Average heights for $p_1 \approx p_{1,c}$ at point 1 (uneasy detachment) in the presence of a barrier, plotted against t .

ansatz

$$\langle n(x, t) \rangle = t^{-\mu} \Phi[(p_1 - p_{1,c})t^{1/\nu_t}] \quad (13)$$

seems to describe the asymptotic behavior. From the scaling of the critical curve we then obtain $\mu = 0.23(1)$, while the scaling of n_∞ against $p_1 - p_{1,c}$ gives $\mu\nu_t = 0.34(1)$ and thus $\nu_t = 1.5(1)$. Notice, however, that these estimates assume that the curvature of the critical curve seen in Fig. 11 does not continue to much higher values of t . If it does continue, then we actually cannot exclude that $\mu = 0$ and the above scaling laws could be all wrong—although we would consider this as extremely unlikely.

If there are scaling laws for $\rho(n, t)$, they should be different for $n = 0$ and $n > 0$. Values of $\rho(0, t)$ are plotted in Fig. 12 for several values of p_1 . We verify again that $p_{1,\text{detach}} = p_{1,c}$, and we see similar FSS as for $\langle n(x, t) \rangle$. But a closer inspection shows that the power law at criticality,

$$\rho(0, t) \sim t^{-\delta}, \quad (14)$$

is actually much less clean than suggested by a fit in the large interval $10^2 < t < 10^7$. While that would suggest $\delta = 0.72(2)$, the data for $t > 10^6$ show a clear deviation which leads to $\delta \leq 0.60(3)$. We cannot, indeed, give any nonzero lower bound on δ with any confidence. From Fig. 12 we can

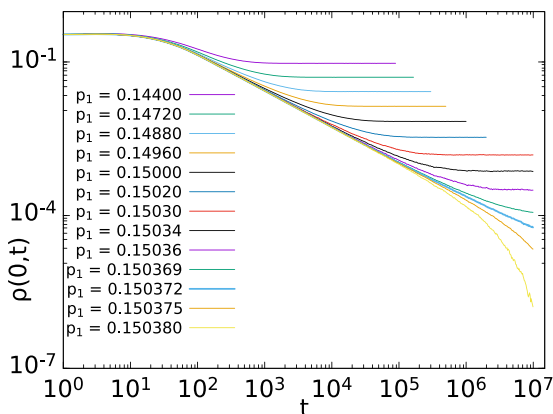


FIG. 12. Fractions of the interface that are at height $n = 0$ for several values of p_1 at point 1 and in the presence of a barrier.

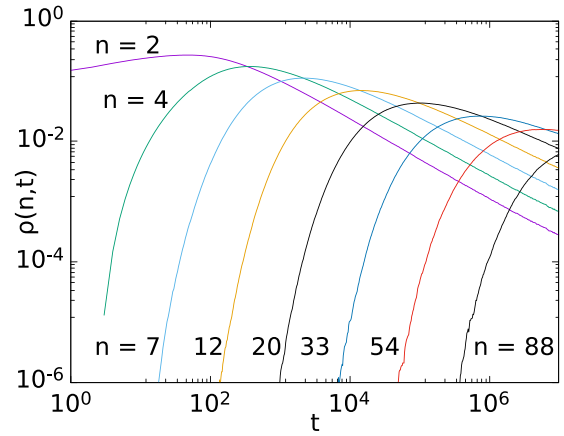


FIG. 13. Fractions of the interface that are at heights $n = 2, 4, 7, 12, \dots, 88$ for $p_1 = p_{1,c}$, at point 1 and in the presence of a barrier.

also read off values of $\rho_{\infty,0} = \lim_{t \rightarrow \infty} \rho(0, t)$ for $p_1 < p_{1,c}$. Again, a casual analysis would suggest a power law $\rho_{\infty,0} \sim (p_{1,c} - p_1)^y$, but a more careful inspection shows that there are so large deviations that we refrain from quoting a value for the exponent y .

For each $n \geq 2$, $\rho(n, t)$ has a maximum at a value $t = t_n$ which increases with n (see Fig. 13). For large n , this increase follows roughly a power law, but again corrections to it are too large to present a reliable estimate of the exponent.

B. Easy detachment

For point 2, a plot similar to Fig. 10 gives $\alpha = 0.47$ and $p_{1,c} = 0.7093304(2)$. At this point, we made exactly the same simulations and plots that we had also made at point 1. The results are shown in Figs. 14–16.

We see from all three figures that corrections to scaling are now even bigger than for uneasy detachment. But, fortunately, in spite of them we can definitely exclude that easy and uneasy detachment are in the same universality class. The clearest indication is from the average heights shown in Figs. 11 and 14. While the former shows for the critical curve a consistent downward curvature, giving thus an upper bound

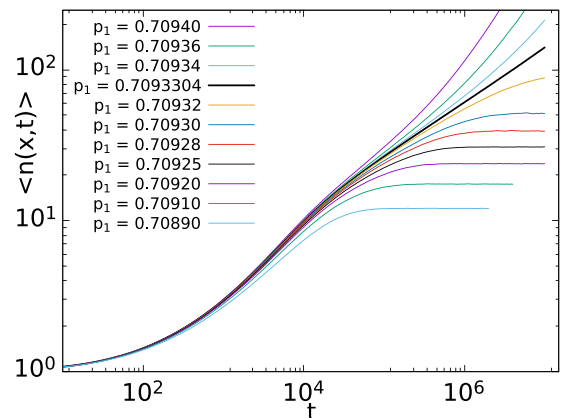


FIG. 14. Average heights for $p_1 \approx p_{1,c}$ at point 2 (easy detachment) in the presence of a barrier, plotted against t .

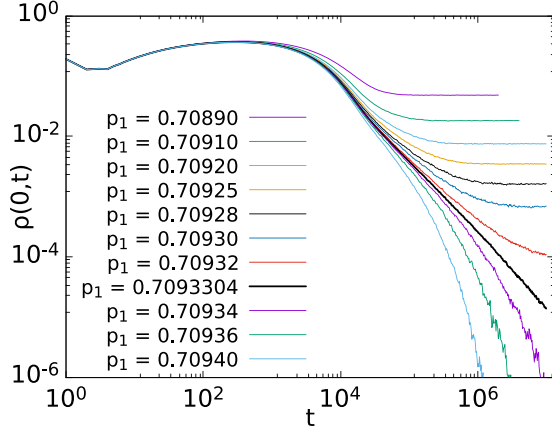


FIG. 15. Fractions of the interface that are at height $n = 0$ for several values of p_1 , at point 2 and in the presence of a barrier.

$\mu \leq 0.23(1)$ for uneasy detachment, the critical curve in Fig. 14 shows for large t an *upward* curvature, giving thus $\mu \geq 0.38(1)$ for easy detachment.

The same conclusion is reached by comparing Figs. 12 and 15. For large t , the critical curve in the former is bent *upward*, leading to $\delta \leq 0.60(3)$, and a careful inspection shows that it is bent *downward* in Fig. 15, giving rise to $\delta \geq 1.24(3)$ for easy detachment.

VI. RELATION TO AVALANCHE PROPAGATION IN THE DIRECTED OSLO MODEL

In sandpile type models, the critical density in the steady state is decided by the requirement that the average height behind a propagating avalanche is same as the average height in front of it. How the avalanches develop when the density is exactly critical depends on details of correlations in the critical background. In the following, we study the propagation of avalanches on specially prepared backgrounds and try to identify when the background becomes critical, and then study the universality classes of this spreading process in a specific case: the directed Oslo rice pile model in two

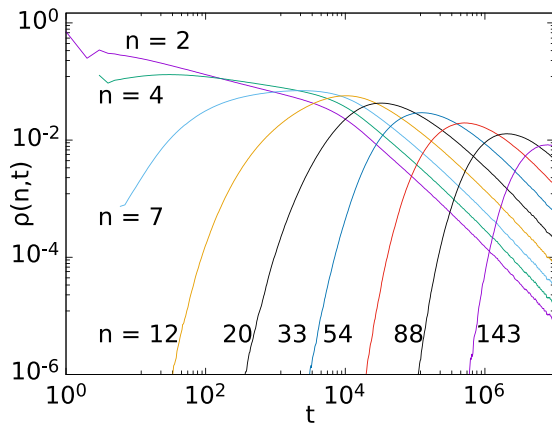


FIG. 16. Fractions of the interface that are at heights $n = 2, 4, 7, 12, \dots, 143$ for $p_1 = p_{1,c}$, at point 2 and in the presence of a barrier.

dimensions [11]. We will show that for a class of specially prepared backgrounds, the avalanche propagation in a version of the directed Oslo rice pile model becomes equivalent to the interface model studied above. The central object of study in the rice pile model [12] is also an interface and its height h , but this is *not* identified with the interface $n(x, t)$. Here we have a two-dimensional square lattice of size $2L \times T$ with periodic boundary conditions in x and open boundary conditions in t . In a stable configuration, each site (x, t) can contain up to two grains of rice. More precisely, call $h(x, t)$ the number of grains at site (x, t) , and define at each site a critical height $h_c(x, t)$. It is initially set for each (x, t) to an independent random value with probabilities $\text{prob}[h_c = 2] = p$ and $\text{prob}[h_c = 3] = 1 - p$. A configuration is stable iff $h(x, t) < h_c(x, t)$ at each site.

Let us start with a random stable configuration, where each site is attributed independently a height 0, 1, or 2 with probabilities c_0, c_1 , and c_2 , with $c_0 + c_1 + c_2 = 1$. Then we add one grain of rice at a randomly chosen x and at $t = 0$. If this leads to an unstable configuration [i.e., if this site then has $h(x, t) \geq h_c(x, t)$], the site *topples*. During a toppling, one grain falls from (x, t) to $(x - 1, t + 1)$, and another from (x, t) to $(x - 1, t + 1)$. This may lead to instabilities at $(x - 1, t + 1)$ or $(x - 1, t + 1)$, which lead then to further topplings and to the evolution of an avalanche. In the usual mode of operation of the model, critical heights at toppling sites are reset randomly (again with probabilities p and $1 - p$), and when an avalanche is finished, a new avalanche starts. Here we modify also this aspect of the model: We randomly reset all critical and actual heights, before a new avalanche starts. Thus each avalanche evolves in a new *uncorrelated* background, with critical height probabilities controlled by p and actual height probabilities controlled by c_i .

We identify $n(x, t)$ in the interface model with the number of topplings in the Oslo sandpile at the site (x, t) . Then $n_{\text{in}}(x, t)$ is the number of grains that come to (x, t) . Clearly, $n(x, t)$ is zero if $n_{\text{in}}(x, t)$ is zero. Now consider the case when $n_{\text{in}}(x, t)$ is odd. Since the site would have zero, one, or two grains, with probabilities c_0, c_1, c_2 , we see that the number of topplings would be $(n_{\text{in}}(x, t) + 1)/2$, with probability $[c_1 p + c_2]$, and otherwise the number is $[n_{\text{in}}(x, t) - 1]/2$. Similarly, if $n_{\text{in}}(x, t)$ is a positive even number, the number of topplings at (x, t) is $n_{\text{in}}/2 - 1, n_{\text{in}}/2, n_{\text{in}}/2 + 1$ with probabilities $c_0(1 - p), c_0 p + c_1 + c_2(1 - p), c_2 p$ respectively. This gives us the identification

$$\begin{aligned} p_0 &= p c_0 + c_1 + (1 - p) c_2, \\ q &= p c_1 + c_2, \\ p_1 &= p c_2. \end{aligned} \quad (15)$$

Notice that the mapping (15) from (c_i, p) to (p_i, q) is neither invertible nor onto. To see the latter, notice that the regions $q < p_1$ and $p_0 + p_1 < q$ do not correspond to any (c_i, p) with $0 \leq c_i \leq 1, 0 \leq p \leq 1$, and $\sum_i c_i = 1$. A more careful analysis shows that this is also true for the whole region $p_0 < 1/2 - (p_1 - p_{-1})^2/2$. For the lack of invertibility, define first

$$r = p_0 + 2p_1 + q. \quad (16)$$

Using Eq. (15) one finds that r can also be written as $r = c_1 + 2c_2 + p$, and that

$$\begin{aligned} q &= p(r - 2c_2 - p) + c_2 \\ &= pr - p^2 + (1 - 2p) \times (p_1/p). \end{aligned} \quad (17)$$

Inserting this into Eq. (16) we obtain then a cubic equation for p ,

$$p^2(r - p) - p(r - p_0) + p_1 = 0. \quad (18)$$

Depending on the values of p_0, p_1 , and q this can have one, two, or three real-valued solutions, from which c_1 and c_2 can be computed by $c_2 = p_1/p$ and $c_1 = r - 2c_2 - p$, except when $p = 0$. In the latter case we have from Eq. (15) $c_2 = q$ and $c_1 = p_0 - c_2$.

The boundary between finite and infinite avalanches in the (c_i, p) space is sketched in Fig. 17(a). It is the surface bounded by the bounding curve ABCDEFA. Avalanches are always finite in the lower left of it, while infinite avalanches can occur in the upper right. The region in the (p_i, q) space onto which the surface spanned by ABCDEFA is mapped is shown in Fig. 17(b) (green and blue areas). The green area is covered three times by the map [i.e., each point is the image of three points in Fig. 17(a)], while the blue area is covered once. Notice that the lines BG, CG, and DG in Fig. 17(a) are all mapped onto the same line $p_1 = p_{-1} = 0$ in Fig. 17(b).

In addition, we have the following comments.

First, along the line AB we have $p = 0$ and therefore $p_1 = 0$, according to Eq. (15). The latter is also true along the line CD, since there $c_2 = 0$. Thus both AB and CD map onto the DK model. Furthermore, in point 1 we have also $c_1 = 0$ and therefore $q = p_0$. As we had seen in Sec. IV B 3, this maps onto directed site percolation.

Second, similarly, one sees that both lines CB and DE correspond to $p_1 = 0$, and thus to the tent transition.

Third, by continuity, it follows that the entire green regions in Fig. 17(a) correspond to DP, while the transition is of tent type in the yellow regions.

Fourth, the lines mG and nG in Fig. 17(b) have two preimages each. One preimage of point “m” is on the line AB, the other is on CD. Similarly, the point “n” has one preimage on DE, the other on BC.

Fifth, let us finally discuss the special case with $c_1=1/2, c_0 = p/2, c_2 = (1 - p)/2$, for any $p \in (0, 1)$. This is precisely the line BGD in Fig. 17(a). On the one hand, it maps into the same line $p_1 = p_{-1}$ in Fig. 17(b) as the line CGF. On the other hand, it can be proven that the steady state of the directed rice pile model in the usual mode of operation (i.e., without the random resetting after each avalanche) is a product state with precisely these probabilities. From Eq. (15) we obtain then

$$q = 1/2, \quad p_1 = p_{-1} = p(1 - p)/2. \quad (19)$$

With these parameters, the background after the avalanche has gone through is statistically equivalent to the initially prepared background, and thus this line corresponds to the SOC state. Thus we see that the interface model with these parameters is mapped *exactly* onto the unmodified directed rice pile model [11].

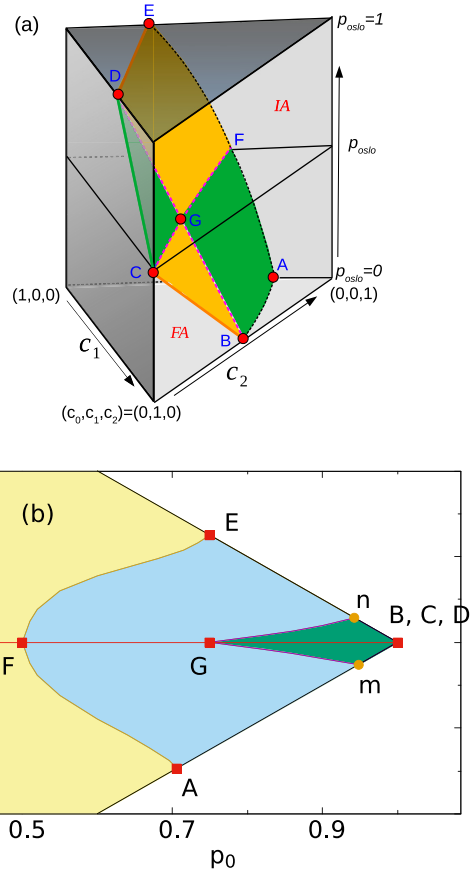


FIG. 17. (a) Rough sketch of the phase portrait of the directed Oslo model. Finite avalanches (“FA”) are left of or below the surface spanned by the bounding curve ABCDEFA, while infinite avalanches (“IA”) can occur to its right or above. The line CGF is precisely at $p = p_{oslo} = 1/2$. On it the model obeys detailed balance, and it is exactly the original directed Oslo model with the original mode of operation, while avalanches evolve always in uncorrelated backgrounds off this line. In the green regions of the critical surface (including the boundary lines AB and CD), the transition is DP, while it is the tent transition in the two yellow regions. More precisely, along the lines AB and CD the model maps onto the DK model, and point A corresponds precisely to directed site percolation. (b) Region in the interface model parameter space onto which the critical surface of panel (a) is mapped. The green region is covered three times by this map, while the blue area is covered once, and the yellow area is not covered at all.

VII. DISCUSSION AND CONCLUSIONS

We have introduced and studied—mostly by numerical simulations—a simple 1D nonequilibrium model that involves three control parameters. As happens in many similar 1D models, it allows for more than one physical interpretation. Indeed, the number of different interpretations is bewildering large, and the number of different critical phenomena which it displays in various regions of control parameter space is fascinating.

The most natural interpretation is as a model for growing interfaces, similar to the famous KPZ model, but with a lower barrier. When the interface hits the barrier it gets stuck to it, and it can detach from it only at the borders (“fronts”) of

the attached regions. In this sense, it is similar to the models in [38–41], but the details are very different. In particular, the activity in [38–41] is in general real-valued, while it is discrete in our model. More specifically, the models in [38–41] can also be formulated as models with multiplicative noise, which is impossible for integer-valued activity.

Another large class of phenomena to which our model bears some resemblance is wetting and dewetting [26,42]. But again, the analogies are far from perfect—mostly because the special discrete nature of our model implies discrete contact angles. Indeed, depending on control parameters, the “liquid” wetting the base (barrier) can have either a flat or a triangle-shaped surface. Nevertheless, our model shows a feature that resembles the distinction between high and low wettability: Lateral spreading of the activity below interfaces that are partially attached to the barrier can be “pulled” or “pushed” [25].

This distinction establishes a relation to another large class of phenomena: Front propagation into unstable states [25]. But it is also of fundamental importance in our model, since we can interpret the model—in the case of pulled fronts, and only then—as a realization of the important contact process (directed percolation) universality class [43]. Thus we have also an immediate relationship with epidemic spreading. But, compared to all previous realizations of epidemic spreading based on the contact process where sites can be only active or inactive, our present realization allows for varying and unbounded local activity. Epidemic spreading with nontrivial local activity levels is one of the basic features of helminth infections [13]. It would be interesting if our model could indeed be applied to them.

While the lateral spreading of attached interfaces is thus related to and relevant for epidemic spreading, the detachment of interfaces from the barrier is most interesting for wetting and multiplicative noise models. In our model, nonattached interfaces are in general of KPZ type, implying that they are typically not symmetric under up or down reflection. More precisely, 1D interfaces of KPZ type can be either noisy concatenations of cup-convex arcs or of cap-convex arcs. We found that this distinction has definitely consequences for the detachment transition: In both cases we found critical behavior (i.e., the transition is continuous), but the two cases are in different universality classes. We reached this conclusion (which is opposite to claims in [39,41], which were, however, made for a similar class of models) in spite of very large corrections to scaling, which made it impossible to give precise estimates for critical exponents. But we could give rather precise bounds such that the upper bounds for one case were lower than the lower bounds for the other.

We should, finally, point out that large scaling corrections are, maybe, the most pervading feature of the present study, and are responsible for most uncertainties that remain. In part, they are not unexpected: Since robust universality classes like the directed percolation class are attractive in the renormalization group (RG) sense, we must expect large cross-over phenomena due to RG flows from other (unstable) fixed points. But this is not all. In addition we found that the expected KPZ scaling for free (nonattached) interfaces sets in very late, due to a special feature of our model [19], namely, that the interface propagation velocity depends periodically on the interface tilt.

There are a number of open questions. One is the precise scaling for the detachment transitions. The other is the precise way that KPZ scaling is reached, in particular when the control parameter q is close to $1/2$, which is also the region where the KPZ scaling should cross over to Edwards-Wilkinson scaling. Due to the latter difficulty, e.g., the scaling for what we called the “clipped KPZ” transition is not yet well understood. But similar uncertainties remain also in other regions of the control parameter space. For instance, the curves in Fig. 1 seem to approach the lines $p_1 = 0$ and $p_1 = 1$ tangentially and merge with them at nontrivial points. Within numerical uncertainty, we cannot, however, exclude the possibility that they meet these lines only at the end point $p_0 = 1$. Another open problem is the precise relationship with the directed Oslo rice pile model sketched in Sec. VI. This relationship is well understood at the symmetry line $q = 1/2$. The other regions of parameter space do not have any direct relationship to the steady-state behavior of the rice pile model.

In this paper, we have dealt with one very specified simplified model, which showed the entire bouquet of fascinating features. But how robust are they? Otherwise said: Are there similar models, either with continuous variables or on other lattices, which display the same features? In particular, do models exist which exhibit most of these features, but without a periodic tilt dependence of interface velocities?

Finally, the last and maybe most difficult open question is whether generalizations exist to higher dimensions with similarly rich behavior.

ACKNOWLEDGMENTS

P.G. thanks the Leverhulme Trust for financial support and the University of Aberdeen, where part of this work was done, for a most pleasant stay. D.D.’s research was supported by a Senior Scientist fellowship by the National Academy of Sciences of India.

-
- [1] L. Reichl, *A Modern Course in Statistical Physics*, 3rd ed. (Wiley-VCH, New York, 2016).
 [2] C. Castellano, S. Fortunato, and V. Loreto, Statistical physics of social dynamics, *Rev. Mod. Phys.* **81**, 591 (2009).
 [3] J.-P. Bouchaud and M. Potters, *Theory of Financial Risk and Derivative Pricing: From Statistical Physics to Risk Management*, 2nd ed. (Cambridge University Press, Cambridge, 2003).

- [4] P. G. de Gennes, *Scaling Concepts in Polymer Physics* (Cornell University Press, Ithaca, NY, 1979).
 [5] N. T. J. Bailey, *The Mathematical Theory of Infectious Diseases and Its Applications*, 2nd ed. (Griffin, London, 1975).
 [6] D. Stauffer and A. Aharony, *Introduction to Percolation Theory*, 2nd ed. (Taylor and Francis, London, 1994).
 [7] P. Grassberger and K. Sundermeyer, Reggeon field theory and Markov processes, *Phys. Lett. B* **77**, 220 (1978).

- [8] J. L. Cardy and R. L. Sugar, Directed percolation and Reggeon field theory, *J. Phys. A: Math. Gen.* **13**, L423 (1980).
- [9] M. Paczuski and S. Boettcher, Universality in Sandpiles, Interface Depinning, and Earthquake Models, *Phys. Rev. Lett.* **77**, 111 (1996).
- [10] P. Bak, C. Tang, and K. Wiesenfeld, Self-Organized Criticality: An Explanation of the $1/f$ Noise, *Phys. Rev. Lett.* **59**, 381 (1987); Self-organized criticality, *Phys. Rev. A* **38**, 364 (1988).
- [11] D. Dhar and R. Ramaswamy, Exactly Solved Model of Self-Organized Critical Phenomena, *Phys. Rev. Lett.* **63**, 1659 (1989).
- [12] V. Frette, K. Christensen, A. Malthe-Sørensen, J. Feder, T. Jøssang, and P. Meakin, Avalanche dynamics in a pile of rice, *Nature (London)* **379**, 49 (1996).
- [13] R. M. Anderson, Population dynamics and control of hookworm and roundworm infections, in *Population Dynamics of Infectious Diseases: Theory and Applications*, edited by R. M. Anderson (Chapman & Hall, London 1982), pp. 67–108.
- [14] *Ascaris lumbricoides*, in Wikipedia, https://en.wikipedia.org/wiki/Ascaris_lumbricoides.
- [15] L. S. Roberts and J. Janovsky Jr., *Foundations of Parasitology*, 8th ed. (McGraw-Hill, New York, 2009).
- [16] M. Kardar, G. Parisi, and Y.-C. Zhang, Dynamic Scaling of Growing Interfaces, *Phys. Rev. Lett.* **56**, 889 (1986).
- [17] S. F. Edwards and D. R. Wilkinson, The surface statistics of a granular aggregate, *Proc. R. Soc. London A* **381**, 17 (1982).
- [18] A.-L. Barabasi and H. E. Stanley, in *Fractal Concepts in Surface Growth* (Cambridge University Press, Cambridge, 1995), pp. 123–125.
- [19] P. Grassberger, Kardar-Parisi-Zhang type dynamics with periodic tilt dependence of the propagation velocity in 1+1 dimensions, [arXiv:2111.11414](https://arxiv.org/abs/2111.11414).
- [20] P. Grassberger, Critical percolation in high dimensions, *Phys. Rev. E* **67**, 036101 (2003).
- [21] P. Grassberger, Logarithmic corrections in (4+1)-dimensional directed percolation, *Phys. Rev. E* **79**, 052104 (2009).
- [22] J. G. Foster, P. Grassberger, and M. Paczuski, Reinforced walks in two and three dimensions, *New J. Phys.* **11**, 023009 (2009).
- [23] J. Wang, Z. Zhou, Q. Liu, T. M. Garoni, and Y. Deng, High-precision Monte Carlo study of directed percolation in ($d + 1$) dimensions, *Phys. Rev. E* **88**, 042102 (2013).
- [24] P. Devillard and H. Spohn, Universality class of interface growth with reflection symmetry, *J. Stat. Phys.* **66**, 1089 (1992).
- [25] W. van Saarloos, Front propagation into unstable states, *Phys. Rep.* **386**, 29 (2003).
- [26] V. M. Starov, M. G. Velarde, and C. J. Radke, *Wetting and Spreading Dynamics* (CRC Press, Taylor & Francis Group, New York, 2007).
- [27] A. Torcini, P. Grassberger, and A. Politi, Error propagation in extended chaotic systems, *J. Phys. A: Math. Gen.* **28**, 4533 (1995).
- [28] J. W. Essam, Directed compact percolation: Cluster size and hyperscaling, *J. Phys. A: Math. Gen.* **22**, 4927 (1989).
- [29] E. Domany and W. Kinzel, Equivalence of Cellular Automata to Ising Models and Directed Percolation, *Phys. Rev. Lett.* **53**, 311 (1984).
- [30] M. Campostrini, M. Hasenbusch, A. Pelissetto, P. Rossi, E. Vicari, Critical exponents and equation of state of the three-dimensional Heisenberg universality class, *Phys. Rev. B* **65**, 144520 (2002).
- [31] N. Clisby, High resolution Monte Carlo study of the Domb-Joyce model, *J. Phys.: Conf. Ser.* **921**, 012012 (2017).
- [32] I. Jensen, Low-density series expansions for directed percolation: I. A new efficient algorithm with applications to the square lattice, *J. Phys. A: Math. Gen.* **32**, 5233 (1999).
- [33] D. Kashchiev, *Nucleation* (Butterworth-Heinemann, Oxford, 2000).
- [34] J. M. Ball, J. Carr, and O. Penrose, The Becker-Doering cluster equations: Basic properties and asymptotic behaviour of solutions, *Commun. Math. Phys.* **104**, 657 (1986).
- [35] J. W. Cahn, Critical point wetting, *J. Chem. Phys.* **66**, 3667 (1977).
- [36] P. Grassberger, L. Chen, F. Ghanbarnejad, and W. Cai, Phase transitions in cooperative coinfections: Simulation results for networks and lattices, *Phys. Rev. E* **93**, 042316 (2016).
- [37] Notice that we would have expected *a priori* an exponent $\alpha = 1/3$; see Ref. [19].
- [38] A. S. Pikovsky and J. Kurths, Roughening interfaces in the dynamics of perturbations of spatiotemporal chaos, *Phys. Rev. E* **49**, 898 (1994).
- [39] M. A. Muñoz, G. Grinstein, and Y. Tu, Survival probability and field theory in systems with absorbing states, *Phys. Rev. E* **56**, 5101 (1997).
- [40] P. Grassberger, Directed percolation: Results and open problems, in *Nonlinearities in Complex Systems, Proceedings of the 1995 Shimla Conference on Complex Systems* (Narosa Publishing, New Dehli, 1997).
- [41] H. Hinrichsen, R. Livi, D. Mukamel, and A. Politi, Model for Nonequilibrium Wetting Transitions in Two Dimensions, *Phys. Rev. Lett.* **79**, 2710 (1997).
- [42] P.-G. de Gennes, F. Brochard-Wyart, and D. Quéré, *Capillarity and Wetting Phenomena* (Springer, New York, 2004).
- [43] H. Hinrichsen, Non-equilibrium critical phenomena and phase transitions into absorbing states, *Adv. Phys.* **49**, 815 (2000).

Correction: Typographical errors in the caption to Figure 17 and in the last sentence of the penultimate paragraph of Sec. VII were introduced during the proof production cycle and have been fixed.